JOURNAL OF COMPUTATIONAL PHYSICS **123,** 169–181 (1996)
ARTICLE NO. 0014

A Grid-Based Coulomb Collision Model for PIC Codes

MICHAEL E. JONES, DON S. LEMONS, RODNEY J. MASON, VINCENT A. THOMAS, AND DAN WINSKE

Applied Theoretical Physics Division, Los Alamos National Laboratory, Los Alamos, New Mexico 87545

Received January 28, 1994; revised March 29, 1995

A new method is presented to model the intermediate regime between collisionless and Coulomb collision dominated plasmas in particle-in-cell codes. Collisional processes between particles of different species are treated through the concept of a grid-based ''collision field,'' which can be particularly efficient for multi-dimensional applications. In this method, particles are scattered using a force which is determined from the moments of the distribution functions accumulated on the grid. The form of the force is such to reproduce the multi-fluid transport equations through the second (energy) moment. Collisions between particles of the same species require a separate treatment. For this, a Monte Carlo-like scattering method based on the Langevin equation is used. The details of both methods are presented, and their implementation in a new hybrid (particle ion, massless fluid electron) algorithm is described. Aspects of the collision model are illustrated through several one- and two-dimensional test problems as well as examples involving laser produced colliding plasmas.

I. INTRODUCTION

Since the earliest days of numerical simulation of plasmas, two fundamental and distinct approaches have been developed to model plasma behavior. One approach has been to consider the plasma as a fluid [1]. In this hydrodynamic, or in the case of a magnetized plasma, magnetohydrodynamic, limit it is assumed that on spatial and temporal scales of interest only the lowest moments of the Boltzmann equation are necessary to describe the dynamics of the plasma. Implicit in this approach is that collisional processes keep the velocity distributions near Maxwellian. An alternative methodology is the kinetic limit, where the individual behavior of the plasma constituents, namely electrons and ions, remains important and, because of the absence of collisional processes, non-Maxwellian features of the particle distribution functions can be significant. Kinetic calculations are usually carried out with particle-in-cell codes [2].

Both techniques have evolved into mature branches of computational physics over the last three decades. Some bridging of the gap between these methodologies can be achieved through the use of hybrid algorithms, where one (typically the electrons) or more plasma constituents are treated as a fluid, while the remaining species are considered in the kinetic limit [3–14], or through the use of Fokker–Planck methods, where the velocity distribution functions are expanded in a set of basis functions (e.g., Legendre polynomials) [15]. Alternatively, multifluid models treat each species as a distinct fluid whose interaction is essentially collisionless [16]. Even so, the distinction between collisionless and collisional plasma interactions has remained essentially intact, except for a few attempts to model Coulomb collisions between different charged particle species and collision processes involving charged particles interacting with neutrals in particle codes (see [17] for a good historical perspective).

In recent years, extensions of old problems as well as new applications have called for the need to examine situations where the plasma is subject to Coulomb collisions that can be regarded as either ''semi-collisional'' or else changing rapidly and continuously in time or space from a strongly collisional state to a collisionless state (or vice versa). In this regime, none of the methodologies discussed above are completely adequate. We briefly describe three areas of current research in this new regime, although many others could be cited as well. The first area involves the interpenetration of laser produced plasmas produced by two laser beams striking a pair of closed spaced targets [18]. For some parameters of the interaction, the two plasmas can couple by classical Coulomb collisions, stagnate between the two targets, and as a result, generate two outgoing shocks [19]. For other parameters, the plasmas can interact through collisionless microturbulent processes (plasma instabilities), or simply stream through each other and not couple at all. Recently, multifluid models [16] and Fokker–Planck methods [15] have been developed to treat these types of interactions, while the collisionless coupling of two plasma streams has been studied previously [20]. A second area of interest concerns the refilling of the Earth's plasmasphere, where magnetic flux tubes con-

* Presently at Department of Physics, Bethel College, North Newton, KS 67117.

0021-9991/96 $12.00

nected to the Earth are opened and vented of plasma during geomagnetic substorms [21]. During more quiet times, the flux tubes become closed and are refilled with plasma from the ionosphere. The refilling process involves the outflow from each hemisphere of collisional ionospheric plasma that becomes collisionless at higher altitudes. These plasmas meet at the magnetic equator and interact there, again through either collisionless or classical collisional processes that are not well understood at present. Both single- and multi-fluid [22] models have been constructed and particle codes [23] have been used to address the issues of plasma flow and interaction in this case. A third area of interest concerns weak instabilities and resulting cross-field transport in inhomogeneous magnetized plasmas, in which Coulomb collisions are not negligible [24]. In recent years, gyro-kinetic [25] and partially linearized (δf) [26] methods have been developed to treat these problems for fusion applications, and collision algorithms that take advantage of the assumptions of these models have been worked out [27, 28].

The issue of modeling collisional processes in particle codes extends back nearly three decades. Early work [29, 30] involved the scattering of particles with a fixed background to model charged particle collisions with neutrals and an understanding of the inherent numerical collisions present in particle codes [31, 32]. The more complex problem of binary Coulomb collisions was addressed in an approximate manner by Oliphant and Nielson [33]. The standard approach to short range Coulomb collisions, however, involves the pairing of scattering particles in each computational cell to ensure that energy and momentum are conserved locally, as originally done by Takizuka and Abe [34]. This method has recently been improved with a vectorized procedure to speed up the process [27] and with a way to collide particles with different numerical weights [35].

The fact that these traditional methods have met with only limited success in addressing problems of multi-species plasmas interacting in a manner, where the collisionality can be a strong function of parameters has led us to seek a new approach. In contrast to previous methods, where the particle collisions are usually treated as encounters between individual pairs of particles or in a more random (Monte-Carlo) manner, in our method collisions between particles of different species are modeled through a "collision field," which is a grid quantity. The properties of the collision field force are chosen so that energy and momentum are conserved locally and that the collision rates reduce to the appropriate (i.e., Spitzer [36]) values for Coulomb collisions. The special case of collisions between particles of the same plasma species (intraspecies collisions) requires a somewhat different treatment, more akin to a Monte-Carlo approach. We will show how the two aspects of the model lead to similar results. The collision model is particularly well suited for multi-dimensional calculations and for interactions involving multiple plasma species.

The plan of this paper is as follows. In Section II the collision field method is introduced. In Section III the case of Coulomb collisions between two different (e.g., ion) species is discussed. The explicit form of the collision field in this case is described and several simple two-dimensional test problems are discussed. The issue of intraspecies collisions is addressed in a similar manner in Section IV, again with appropriate test problems. A more complex application of colliding laser produced plasmas is considered in Section V, involving mostly one-dimensional calculations but including a 2D case and an example with multiple ion species. A summary and conclusions are given in Section VI. For the cases discussed here, the collision model is incorporated in a new multi-dimensional hybrid (particle ions, massless fluid electron) code that retains radiation effects. For completeness, the basic equations of this hybrid algorithm are presented in Appendix A.

II. COLLISION FIELD METHOD

The primary desideratum for a self-consistent scattering model is local momentum and energy conservation. In the case of scattering from a fixed background, the reaction of the background is not needed, so the usual random number based Monte Carlo scattering may be used [17, 29, 37]. However, if the self-consistent scattering of two or more species is required, random scattering in which the scattering species is treated as a fixed background will not conserve momentum and energy unless a very large number of particles is used. An alternative approach that has been often employed is to sort the particles and perform scattering in pairs to conserve momentum and energy [34]. The sorting process can be time consuming, although recently developed vectorized methods [27] suggest that perhaps this is no longer a significant issue, and the prescription by which particles are paired together is somewhat arbitrary. This approach is also used, for example, in molecular dynamics to describe the interactions [38]. In general, particles are seldom exactly in the same location at a given time step, so the decision of when to scatter is also not clear. Lattice gas algorithms resolve this problem by requiring all the particles move at the same speed [39]. Non-energy conserving algorithms for modeling galaxy formation have also been devised [40].

A different approach to modeling collisions between particles of different species is adopted here. It is a natural extension of the particle-in-cell method and is an improvement on our earlier work in this area [41]. As usual, the electric and magnetic forces between charged particles can be divided into two parts: long range forces that involve the interaction between particles that are farther than a cell apart ($\Delta x \geq$ electron Debye length) that are treated

through the macroscopic electromagnetic fields and short-range forces involving particles in the same cell. The essence of the method introduced here involves defining a mesh quantity for the short-range collision operator that can be viewed as a "collision field." This field mediates the collision force and is defined such that it yields local conservation of momentum and energy. Similar collision operators with local conservation properties have been recently developed for δf simulations [28].

We define $\mathbf{F}_{\alpha\beta}$ as the force on a particle of species α due to collision with the particles of species β. Momentum conservation requires

$$\langle \mathbf{F}_{\alpha\beta} \rangle = -\langle \mathbf{F}_{\beta\alpha} \rangle, \tag{1}$$

where the brackets denote distribution function averages. For particle-in-cell codes, these averages are functions of the fluid quantities obtained by interpolating particle information onto the grid. We also require that the short range collision force conserve energy locally so that

$$\langle \mathbf{v}_\alpha \cdot \mathbf{F}_{\alpha\beta} \rangle = -\langle \mathbf{v}_\beta \cdot \mathbf{F}_{\beta\alpha} \rangle. \tag{2}$$

where $\mathbf{v}_\alpha$ is the velocity of a single particle of species α. The collision field method then involves finding an appropriate form for the force, $\mathbf{F}_{\alpha\beta}$, which satisfies Eqs. (1) and (2). In the next section, the form of the force for collisions between two different particle species ("interspecies collisions") is presented. The related, but distinct issue of how to treat collisions within the same particle species ("intraspecies collisions") is considered in Section IV.

III. INTERSPECIES COLLISIONS

We first consider the collision force between two distinct species, α and β. For multiple species, earlier work in this area [19, 42] assumes that each species can be treated as a separate fluid. The transport equations then involves coupling of the momentum and energy moments of each fluid. A rigorous analysis of fluid transport equations derived from the Boltzmann equation for two or more species has recently been carried out by Decoster [43]. He assumes that each species consists of a drifting Maxwellian and finds that the transport equations give rise to two collision frequencies. In this approximation, the fluid equations that couple two species together can be written as

$$n_\alpha m_\alpha \frac{d}{dt} \langle \mathbf{v}_\alpha \rangle = \mathbf{R}_{\alpha\beta} + ... \tag{3}$$

$$\frac{3}{2} n_\alpha \frac{d}{dt} T_\alpha = Q_{\alpha\beta} + ..., \tag{4}$$

where

$$\mathbf{R}_{\alpha\beta} = -\nu_{\alpha\beta} n_\alpha m_{\alpha\beta} (\langle \mathbf{v}_\alpha \rangle - \langle \mathbf{v}_\beta \rangle) \tag{5}$$

and

$$Q_{\alpha\beta} = \frac{m_{\alpha\beta}}{m_\alpha} \mathbf{R}_{\alpha\beta} \cdot (\langle \mathbf{v}_\alpha \rangle - \langle \mathbf{v}_\beta \rangle) - \nu^\varepsilon_{\alpha\beta} n_\alpha (T_\alpha - T_\beta). \tag{6}$$

and the ... correspond to the rest of the terms in the fluid equations that depend only on species α. Here, n_α, T_α, and m_α are the density, temperature, and mass of species α. The two collision frequencies, $\nu_{\alpha\beta}$ and $\nu^\varepsilon_{\alpha\beta}$ are given by

$$\nu_{\alpha\beta} = \frac{8\sqrt{\pi}\, Z_\alpha^2 Z_\beta^2 e^4 n_\beta \ln \Lambda_{\alpha\beta}}{m_{\alpha\beta}^2 (\Delta v)^3} \left[\frac{\sqrt{\pi}}{2} \operatorname{erf}\left(\frac{\Delta v}{v_{th}}\right) - \left(\frac{\Delta v}{v_{th}}\right) \exp\left(\frac{-\Delta v^2}{v_{th}^2}\right) \right] \tag{7}$$

and

$$\nu^\varepsilon_{\alpha\beta} = \frac{16\sqrt{\pi}\, Z_\alpha^2 Z_\beta^2 e^4 n_\beta \ln \Lambda_{\alpha\beta}}{m_\alpha m_\beta v_{th}^3} \exp\left[-\left(\frac{\Delta v}{v_{th}}\right)^2 \right] \tag{8}$$

where $v_{th}^2 \equiv 2(T_\alpha/m_\alpha + T_\beta/m_\beta)$ and $\Delta v \equiv |\langle \mathbf{v}_\alpha \rangle - \langle \mathbf{v}_\beta \rangle|$, the reduced mass $m_{\alpha\beta} \equiv m_\alpha m_\beta/(m_\alpha + m_\beta)$, $\ln \Lambda_{\alpha\beta}$ is the Coulomb logarithm, with $Z_\alpha e$ the charge on the ion of species α, and erf is the error function. Evidently, the collision frequency $\nu_{\alpha\beta}$ in (7) is a dynamic friction, while $\nu^\varepsilon_{\alpha\beta}$ in (8) is related to temperature equilibration. If the velocity distribution is near Maxwellian, the dynamic friction given by Eq. (7) will yield the correct relaxation rate. Usually, we assume that $\ln \Lambda_{\alpha\beta}$ is a constant, although one can, of course, calculate it locally or include a maximum impact parameter (minimum scattering angle) that depends on the cell size.

These expressions can be compared with those commonly used in multifluid [16, 19] and Fokker–Planck [15] calculations of colliding plasma experiments. The expressions used by Berger *et al.* [19] have been updated with an analytic correction based on Decoster's [43] treatment (which is included exactly in our Eqs. (7)–(8)) and is given in Ref. [15, Eq. (13)]). That expression (for $m_\alpha = m_\beta$) agrees exactly with Eq. (7) in the limits $\Delta v/v_{th} \ll 1$ and $\gg 1$ and is about 30% smaller than (7) for $\Delta v/v_{th} = 1$. However, for $m_\alpha \neq m_\beta$, one must be careful as the reduced mass in Eq. (13) of Ref. [15] and Eq. (18) of Ref. [19] are not explicitly denoted. In addition, unlike (7) and (8), the expressions for $\nu^\varepsilon_{\alpha\beta}$ in Refs. [15, 16, 19] are identical to those for $\nu_{\alpha\beta}$, except for a constant ($\sim$4 for $m_\alpha = m_\beta$). While this agrees with Eq. (8) for $\Delta v/v_{th} \leq 1$, in the limit $\Delta v/v_{th} \gg 1$, it gives a much larger value than Eq. (8),

which has an extra exponential factor. Because both collision frequencies, (7) and (8), contribute to the heating (Eq. (6)), it is not easy to determine a priori how much accuracy is sacrificed using an approximate form for $\nu^{\varepsilon}_{\alpha\beta}$ rather than Eq. (8).

We consider the following functional form for the collision field:

$$\begin{aligned}\mathbf{F}_{\alpha\beta} = {} & \nu_{\alpha\beta} m_{\alpha\beta}(\langle \mathbf{v}_\beta \rangle - \langle \mathbf{v}_\alpha \rangle) \\ & - \nu_{\alpha\beta} \frac{m^2_{\alpha\beta}}{m_\alpha} \frac{(\langle \mathbf{v}_\beta \rangle - \langle \mathbf{v}_\alpha \rangle)^2}{\langle \mathbf{v}^2_\alpha \rangle - \langle \mathbf{v}_\alpha \rangle^2} (\langle \mathbf{v}_\alpha \rangle - \mathbf{v}_\alpha) \\ & + \nu^{\varepsilon}_{\alpha\beta} \frac{(T_\alpha - T_\beta)}{\langle \mathbf{v}^2_\alpha \rangle - \langle \mathbf{v}_\alpha \rangle^2} (\langle \mathbf{v}_\alpha \rangle - \mathbf{v}_\alpha).\end{aligned} \tag{9}$$

It is easily shown that the form of the force in Eq. (9) satisfies Eqs. (1) and (2) for local, instantaneous momentum and energy conservation. It also reproduces both fluid transport equations, Eqs. (3) and (4), when averaged over the particle distribution. Given the simplifying, but essentially arbitrary, assumption that the force on a particle of species α is a linear function of these constraints, i.e., Eqs. (3)–(4), the particle velocity completely determines the force (9). It should also be noted that other types of elastic collisions could be treated by this method, with different expressions for the collision frequencies. The collision field method could, in principle, also be applied to other kinds of collisions, by changing the form of the force (9), e.g., inelastic collisions by relaxing (2).

The numerical implementation of these equations is straightforward. The fluid quantities, n_α, $\langle \mathbf{v}_\alpha \rangle$, T_α, etc. are obtained by linear interpolation onto the grid from the particle quantities. Given these mesh quantities, the collision field is also evaluated on the grid. When the particles are moved during the next time step, the effect of the collision force is included with the Lorentz force in updating the particle velocities.

The method as presented is not limited to small collision rates and, in fact, has been formulated so that a wide range of collisions can be addressed in the same calculation. Some caution, however, must be used in the limit of large collision frequencies ($\nu_{\alpha\beta}\Delta t > 1$), where a particle experiences more than one collision per time step. In this case, we simply limit the collision rate to a fraction (typically 0.5) of the inverse time step. This has the effect of following the dynamics of the plasma on the slower scale, with the approximation that the collision rate is large enough to drive the system to equilibrium in a few time steps, rather than one time step. An extension of the method in which the collisions are treated implicitly overcomes this difficulty and will be discussed in a future publication. It should also be noted that the same formulation discussed here for ion–ion collisions is used to calculate the force on the ions from the electrons, except the electron density, velocities, and temperature are already fluid grid quantities. As shown in the Appendix, the corresponding force of the ions on the electrons is included in the electron momentum equation that is used to solve for the electric field.

We consider two test problems to demonstrate the utility of the interspecies collision model. The first example involves the thermal relaxation of two ion populations with different densities and initial temperatures at rest with respect to each other ($n_1 = 0.1 n_2$ with temperatures $T_1 = 4T_2$ and thermal speed $v_{th1} = (2T_1/m_1)^{1/2}$). This problem has been considered by Rambo and Procassini [44], and we use their parameters here: $n_1 = 10^{19}$ cm^{-3}, $T_1 = 1$ keV, with $Z_\alpha = Z_\beta = 6$, $m_\alpha = m_\beta = m_p$ (proton mass) and $\ln \Lambda_{\alpha\beta} = 10$. The corresponding collision frequency is $\nu^{\varepsilon}_{\alpha\beta} = 4.9 \times 10^{12}$ s^{-1}. The simulation is done in the r, z plane, with the plasma inside a radius $R = (r^2 + z^2)^{1/2} = 500\ \mu$m, with 1792 computational cells and 62500 macroparticles; the time step is 0.005 ps. The self-consistent electric and magnetic fields have been turned off in the calculation so that only collisional interactions occur. Figure 1a shows the velocity distribution (velocities normalized to v_{th1}) at $t = 0$ (top panel) and $\nu^{\varepsilon}_{\alpha\beta} t = 9.8$ ($t = 2.0$ ps) (bottom panel). The denser, initially colder ion distribution is shown as the dotted curves; the initially hotter distribution is given by the solid curves. By $\nu^{\varepsilon}_{\alpha\beta} = 9.8$, the temperatures of two distributions have equilibrated. Figure 1b displays the time history of the temperature of the initially hotter distribution, showing its relaxation to a lower temperature. The solid circles correspond to the fluid solution that can be obtained analytically [44]; overall there is excellent agreement. The open circles correspond to the Monte-Carlo model of Ref. [44], which is argued does not match the fluid solution because of the smaller collision rate of ions in the tail of the distribution. Note that our model, which is also a particle representation, is adjusted so that the correct fluid behavior is reproduced and the particles are scattered at the overall proper rate.

The second test case also involves the collisional interaction of two ion populations with properties similar to the first case, but with a relative drift between them. In this case, the temperatures of both ion populations are equal, $T_1 = T_2 = 0.5$ keV, and $V_1 = 6.5 \times 10^7$ cm/s, $V_2 = 0$; here, the collision frequency is $\nu_{\alpha\beta} = 7.8 \times 10^9 \text{s}^{-1}$. The simulation is done in the same geometry with the same number of particles as before, with a time step of 0.5 ps. Figure 2a shows the ion distributions for this case at three times: $t = 0$, $\nu_{\alpha\beta} t = 0.16$, and finally, $\nu_{\alpha\beta} t = 0.48$ ($t = 60$ ps), when the two populations have relaxed to the same speed. Note that at the intermediate time that the drifting population is heated and remains Maxwellian. The ''heating'' is due to the need to maintain overall energy conservation; by $\nu_{\alpha\beta} t = 0.48$, the distribution has cooled off. The Maxwellian shape of the distribution is again a requirement of the model and is in contrast to the kinetic calculations [44], in

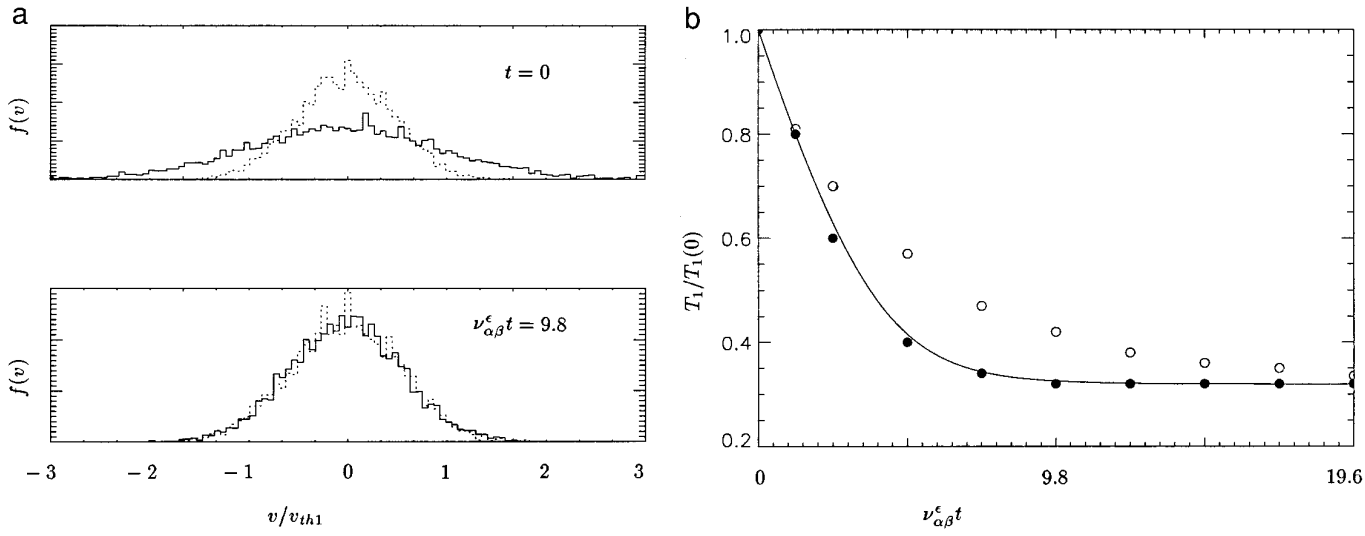

FIG. 1. Interspecies collision test problem showing relaxation of two ion components with different densities and initial temperatures: (a) velocity distributions at $t = 0$ and $\nu^{\epsilon}_{\alpha\beta}t = 9.8$; (b) temperature of the hotter distribution as a function of time. The solid circles are fluid calculations, the open circles are kinetic calculations from [44].

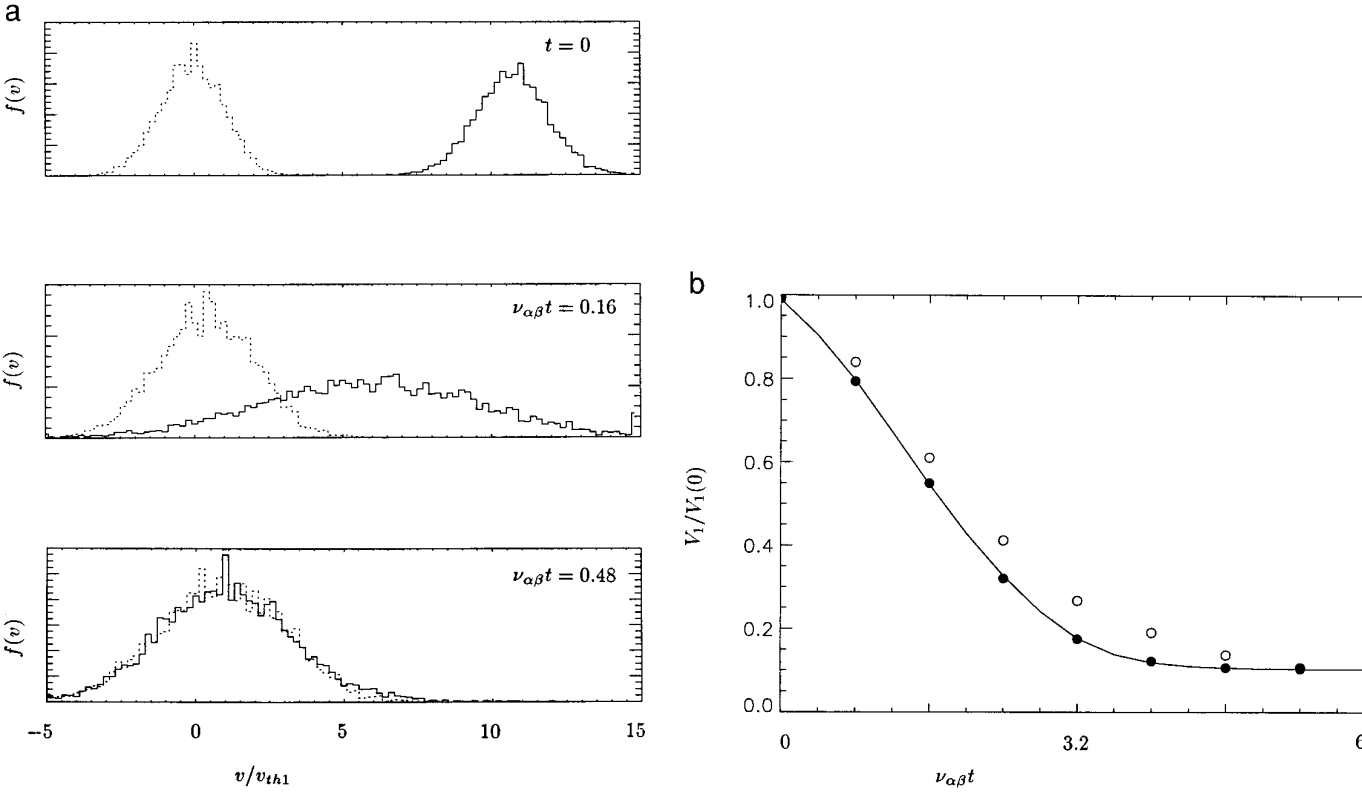

FIG. 2. Interspecies collision test problem showing relaxation of two ion components with different densities and a relative drift: (a) velocity distributions at $t = 0$, $\nu_{\alpha\beta}t = 0.16$ and $\nu_{\alpha\beta}t = 0.48$; (b) velocity of the drifting distribution as a function of time. The solid circles are fluid calculations, the open circles are kinetic calculations from [44].

which significant deviations from Maxwellian behavior can occur at intermediate times. The time history of the velocity of the initially drifting ion component is shown in Fig. 2b. As in Fig. 1b, we also show the fluid results as solid circles and the kinetic solution as open circles [44]. Again, the present calculations reproduce the fluid results quite closely, but deviate from the kinetic solution (which relaxes at a somewhat slower rate).

IV. INTRASPECIES COLLISIONS

In addition to scattering between different plasma species, Coulomb collision processes also occur between particles of the same species. Such collisions tend to relax the velocity distribution to an isotropic Maxwellian. This process cannot be modeled with the collision force field method developed for interspecies collisions, as it is evident from Eq. (9) that $F_{\alpha\beta} = 0$ when $\alpha = \beta$. However, it is well known from the theory of Brownian motion [45] that the Langevin equation is a useful approach to modeling collisions between particles of the same species. As a generalization of that equation, consider the following form of the force

$$\mathbf{F}_{\alpha\alpha}/m_\alpha = -\nu_\alpha(\mathbf{v}_\alpha - \langle \mathbf{v}_\alpha \rangle) + \mathbf{A}, \tag{10}$$

where $\mathbf{A}$ is a random, isotropic vector chosen to provided thermalization and ν_α is a dynamical friction related to the fluid collision frequency.

It is clear that this form of the force conserves momentum, because $\langle \mathbf{F}_{\alpha\alpha} \rangle = 0$, at least in a statistical sense, because the random vector $\mathbf{A}$ has the property $\langle \mathbf{A} \rangle = 0$ and the first term vanishes upon averaging, by definition. Momentum conservation implies that $\langle \mathbf{v}_\alpha \rangle$ does not change. Thus, one can transform into the fluid frame and apply the analysis of Chandrasekhar [45] for the Langevin equation. Letting $\mathbf{v} \equiv \mathbf{v}_\alpha - \langle \mathbf{v}_\alpha \rangle$ and integrating the equation of motion for a particle, we get

$$\Delta \mathbf{v} = -\nu_\alpha \Delta t \mathbf{v} + \mathbf{A}^*, \tag{11}$$

where $\mathbf{A}^* = \int_t^{t+\Delta t} dt' \mathbf{A}(\mathbf{t}')$. The assumption here is that the rate of random collisions associated with $\mathbf{A}^*$ is much greater than the collision rate ν_α associated with the dynamical friction; i.e., the particles experience many small angle scatterings. Chandrasekhar showed that when each particle's velocity is advanced with Eq. (11), the distribution of velocities approaches a Maxwellian for a proper choice of $\mathbf{A}^*$. That is,

$$\lim_{t\to\infty} f(\mathbf{v}, t) = \left(\frac{m_\alpha}{2\pi T_\alpha}\right)^{3/2} \exp\left(-\frac{m_\alpha v^2}{2T_\alpha}\right), \tag{12}$$

provided the $\mathbf{A}^*$ is distributed according to the function $P(A^*)$, where

$$P(A^*) = \left(\frac{m_\alpha}{4\pi \nu_\alpha \Delta t T_\alpha}\right)^{3/2} \exp\left(-\frac{m_\alpha \mathbf{A}^* \cdot \mathbf{A}^*}{4\nu_\alpha \Delta t T_\alpha}\right) \tag{13}$$

for all times. The parameter T_α is the final temperature. Because $\mathbf{A}^*$ is an isotropic vector; i.e., $\langle \mathbf{A}^* \rangle = 0$, momentum is conserved, while the magnitude of $\mathbf{A}^*$, i.e., $(\langle \mathbf{A}^* \cdot \mathbf{A}^* \rangle)^{1/2}$, is such that energy is conserved when Δt is not too large or otherwise chosen appropriately. Specifically,

$$\langle \mathbf{A}^* \cdot \mathbf{A}^* \rangle = 6\nu_\alpha \Delta t T_\alpha / m_\alpha, \tag{14}$$

where $3n_\alpha T_\alpha/2$ is the final energy density of the distribution and thus the total energy in the particles. Then expressing Eq. (11) as a central finite difference equation

$$\mathbf{v}^{n+1} = \mathbf{v}^n - \frac{\nu_\alpha \Delta t}{2}(\mathbf{v}^{n+1} + \mathbf{v}^n) + \mathbf{A}^*, \tag{15}$$

it is straightforward to show using Eq. (14) that

$$\frac{m_\alpha \langle (\mathbf{v}^{n+1})^2 \rangle}{2} = \frac{m_\alpha \langle (\mathbf{v}^n)^2 \rangle}{2} = \frac{3T_\alpha}{2}. \tag{16}$$

In other words, this algorithm conserves energy exactly for any size Δt as long as the averaging process denoted by the brackets $\langle\ \rangle$ is adequately modeled.

The dynamical friction transport coefficient, ν_α, can be taken as the Spitzer [36] value. However, as discussed in the previous section on interspecies collisions, a more accurate method is to calculate the transport coefficients for two drifting Maxwellians. We then take the limit of Eq. (7) as the relative drift vanishes to obtain

$$\nu_\alpha = \frac{4\sqrt{\pi}}{3} \frac{n_\alpha Z_\alpha^4 e^4 \ln \Lambda_{\alpha\alpha}}{m_\alpha^2 (T_\alpha/m_\alpha)^{3/2}}, \tag{17}$$

which is then used in Eq. (15), along with the random vector $\mathbf{A}^*$ (determined from Eq. (13)). It should also be noted that in Eqs. (12)–(14), (16)–(17), T_α, n_α, and hence ν_α are generally functions of space (and time); i.e., the effect of strong spatial gradients are inherently included.

This form of the force ensures that the particle distribution function evolves toward a Maxwellian. Again, one has to check on the magnitude of the collision frequency. If the collision rate is high enough, the net effect of collisions will be that the distribution function is instantaneously Maxwellian and does not change. In practice, we do a crude check on the distribution function. If the distribution is close to Maxwellian, we skip the intraspecies collision

part of the velocity update on that time step. Also, if the collision rate is very large, we limit it, as before, to a fraction of the inverse time step. The large collision frequency limit can be problematic, however, as the temperature of the distribution can slowly drift in time (usually to lower temperatures). This effect has been discussed in detail by Lemons *et al.* [46]. In practice, we have found that the best solution is to do the intraspecies collision part of the particle push first and then renormalize the velocity distribution to conserve energy, followed by the interspecies collision operation. This necessitates going through the particle table twice each time step. Along with the need to collect additional moments for the collision force, it means that the overhead of modeling collisions in the code is about 50% of the total run time. Some of the cost can be recovered by saving some of the moments rather than recomputing them. In addition, because one does not have to resolve each individual collision in the collision field method, the use of larger time steps can reduce the overall cost of the calculation considerably.

To illustrate the intraspecies collision scattering model, we again consider two test problems. The first problem involves the relaxation of an initially square velocity distribution ($f(v_i) = \text{const}$, $|v_i| \leq v_{th}$; $= 0$ otherwise, $i = r, \theta, z$) toward a Maxwellian. This test problem has been used previously to determine the numerical collision frequency in (collisionless) particle codes [31, 32] as a function of the number of particles in a Debye length. Instead, here we allow the distribution to relax via Coulomb collisions between the particles. The simulation parameters are: $n_1 = 10^{20}$ cm^{-3}, $T_1 = 29$ eV, with $Z_\alpha = 1$, $m_\alpha = m_{\text{proton}}$, and $\ln \Lambda_\alpha = 6$. There is only one ion species (about 30000 particles), with velocities spread evenly between $-1 < v_i/v_{th} < 1$. Time is expressed in terms of the corresponding collision frequency, ν_α ($=3 \times 10^9$ s^{-1}), (Eq. (17)). The left panels of Fig. 3 show phase space ($v_z - v_r$) at $t = 0$ and $\nu_\alpha t = 0.053$, indicating the initial cube distribution rapidly evolves into a sphere. The top right panel of Fig. 3 shows the initial z-velocity reduced distribution ($f(v_z)$) as a dotted line; the distribution at $\nu_\alpha t = 0.053$ is plotted as the solid line. Evidently, the distribution has evolved to a near-Maxwellian by this time.

In contrast to the intraspecies collision model used here, our initial form for such collisions [41] and the scattering algorithm of Cranfill *et al.* [47] both use a random rotation of the velocity vector. While this procedure does randomize the velocity distribution, it does not allow particles to attain the large velocities found in the tail of a Maxwellian, as occurs in present method illustrated in Fig. 3. To compare the relaxation rate in the simulation with Eq. (17), we have computed the entropy function, $E(t) = -\int f(v) \ln f(v)\, dv \simeq -3 \int f(v_z) \ln f(v_z)\, dv_z$, assuming $f(v) \simeq f(v_x) f(v_y) f(v_z)$. The bottom panel of Fig. 3 shows the time history of E, with time given in terms of $\nu_\alpha t$, from which

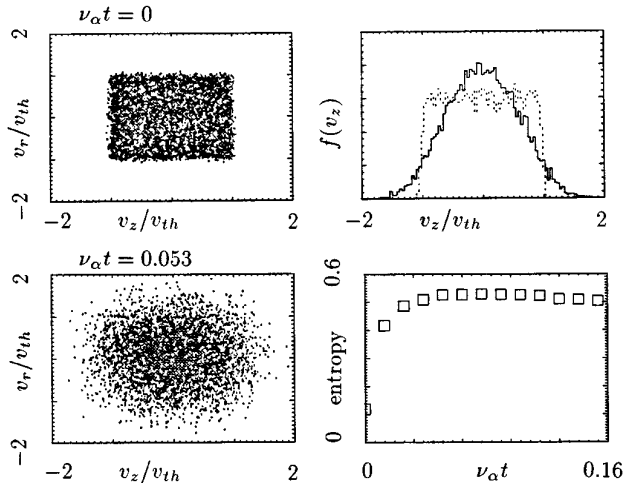

FIG. 3. Intraspecies collisions test problem showing the relaxation of an initially square velocity distribution to a Maxwellian: (left panels) $v_z - v_r$ phase space at $t = 0$ and $\nu_\alpha t = 0.053$; (top right panel) distribution functions (solid curve, $\nu_\alpha t = 0.053$; dotted curve, $t = 0$); and (lower right) corresponding time history of the entropy.

the relaxation time when E first reaches its final value, $\nu_\alpha \tau \simeq 0.05$, can be determined. Evidently, the relaxation for this distribution proceeds quite rapidly in comparison to the theoretical rate, ν_α.

The second test problem for intraspecies collisions involves the flow of a dense fluid toward a stationary wall. Due to the strong collisions, the fluid is heated by the interaction with the wall and an outward propagating shock is formed. This problem has been discussed at length by Noh [48], who provides analytic solutions and comparisons with results obtained from a number of fluid codes. Because of artificial viscosity employed in many fluid algorithms, the heating at the wall is excessive, leading to a density deficiency at the wall. We have simulated this problem in various geometries (planar, cylindrical, spherical) and obtained very good agreement with the analytical solutions. Figure 4 shows the results for spherical geometry, with 100 computational cells and 1000 particles per cell initially. The solid curve is the analytic result at $t = 0.6$ when the shock reaches $r/r_o = 0.2$. Plotted in the top panel is the density; the corresponding temperature is shown in the bottom panel (both normalized to their initial, upstream values). The dashed and dotted curves correspond to the simulation results at the same time. The calculation gives a downstream density of 64 on the average, consistent with the analytic theory. The fluctuations in the calculations decrease with a larger particle number, as expected. The correct shock speed is also reproduced. The temperature profile is also accurately modeled, with somewhat greater spread at the shock front due to the cell averaging used to compute the temperature. The magnitudes of the density and temperature jumps across the shock and the

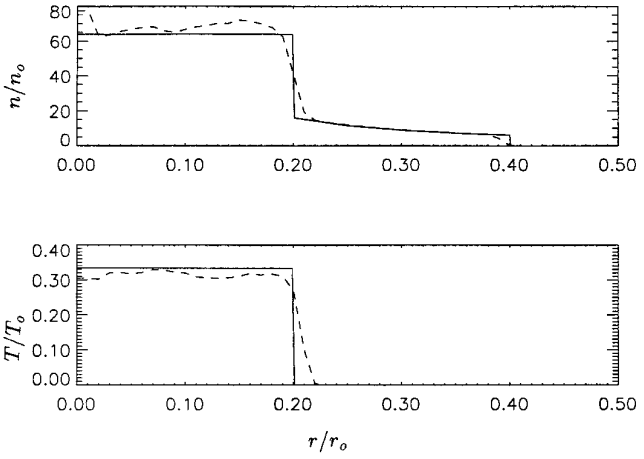

FIG. 4. Spherical Noh problem showing density (top) and temperature (bottom); calculations are plotted as dashed lines, while solid curves are the analytic results.

shock speed also depend slightly on the size of the time step ($\Delta t = 0.4$ here) and the limiting value of the collision rate ($\nu_\alpha \Delta t \leq 0.6$ here).

V. INTERPENETRATION OF LASER PRODUCED PLASMAS

In order to show the usefulness of the collision-field method on a more realistic problem, we consider the interaction of two colliding laser produced plasmas. The physics of the process has been discussed in detail by Berger *et al.* [19] and experiments have been carried out by Bosch *et al.* [18]. These papers should be consulted for the details of how the plasmas are produced and the interaction diagnosed. For our purpose here, one can imagine two heated thin slabs of plasma separated by a finite distance. The plasmas expand isothermally outward from each slab and interact in the region between the slabs. Depending on parameters, the two plasma streams can interact strongly on initial contact to form a stagnated region or can interact weakly and interpenetrate for some distance before coupling together. The limiting cases have been discussed in Ref. [19], by Rambo and Denavit [16] who studied the intermediate regime as well using a multifluid code that includes electron dynamics, by Larroche [15] who employs an ion Fokker–Planck technique to compare with both other calculations [19] and experiments [18], and by Rambo and Procassini [44] who compared fluid and Monte Carlo calculations. We consider a similar situation with parameters roughly corresponding to those used in [19] to investigate various aspects of the collision-field model. In these calculations, we include both short-range interspecies and intraspecies Coulomb collisions, as well as long-range collisions through the self-consistent electric field (Eq. (A.2)).

Experimentally, the initial configuration consists of two thin (200 μm) slabs of gold ions ($A = 197$, $Z_i = 50$) with initial electron density of 3×10^{22} cm^{-3} separated by 1600 μ The electron temperature is held fixed at 2.5 keV. The corresponding model calculations are done in one dimension, with 12000 macroparticles to represent the ions in each slab and a grid of 200 computation cells. Figure 5 shows the phase space (p_z-z) evolution of the two ion species (where p_z is the canonical momentum normalized to the speed of light and the electron rest mass). Figure 5a shows the initial configuration: ions in the two slabs at rest with an initial temperature $T_i = 15$ eV. Figure 5b shows the system at $t = 0.6$ ns. Because of the isothermal nature of the expansion, the fastest ions have propagated further and at this time have not yet begun to interact with the leading edge of the other ion species. Figure 5c shows that at $t = 1.2$ ns the two ion species have interpenetrated and begun to heat and slow down relative to each other, over an interaction region of about 1000 μm. By $t = 1.8$ ns in Figure 5d, the two plasmas are thermalized in the central region. The resulting ion velocity spread is somewhat smaller than in the preceding panel, because of both the ion coupling as well as cooling to the electrons. Figure 6 shows the corresponding plot of the electron density, $n_e = \sum n_i Z_i$ at various times. The buildup of the density between the two target plasmas is comparable to that seen in the Berger *et al.* calculations [19], but by $t = 1.8$ ns, when the two plasmas have interacted strongly, there is no noticeable pileup of the density. Note also that the interactions here involve only Coulomb collisions. The cell sizes and time steps used in the calculations preclude the excitation of short wavelength instabilities and corresponding anomalous collision processes, such as those discussed in Ref. [19].

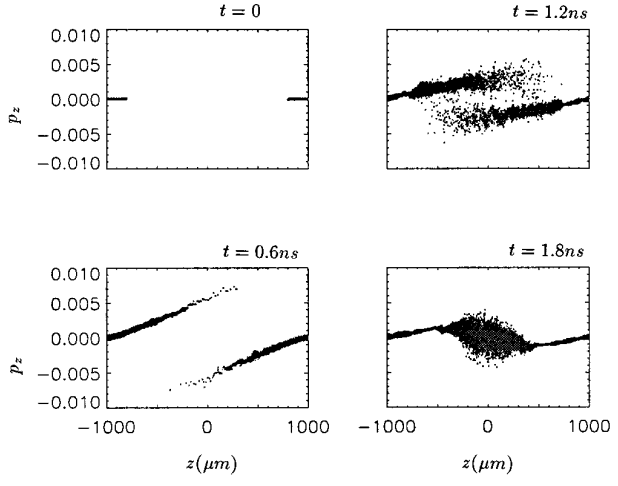

FIG. 5. Interaction of two expanding (laser produced) plasmas, showing ion $p_z - z$ phase space at four times (parameters given in the text) for a one-dimensional calculation.

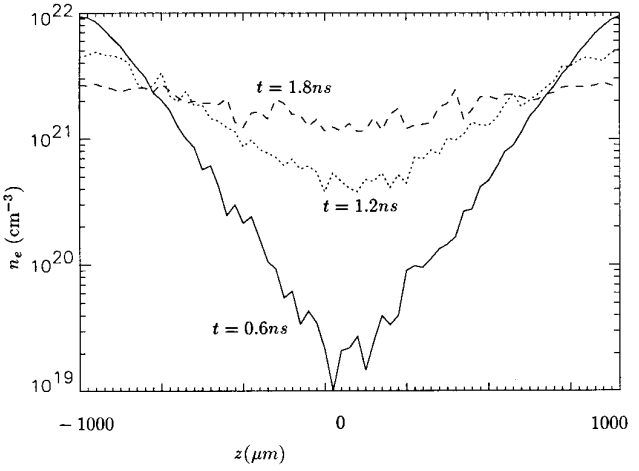

FIG. 6. Profiles in z of the electron density at three times for the same run as in the previous figure.

In expansions of this type, the typical ion streaming velocity is several times the sound speed, $c_s = (ZT_e/m_i)^{1/2}$. Using this expression and Eq. (7), the ion mean free path, $\lambda_{ii} = V_i/\nu_{\alpha\beta}$, is thus

$$\lambda_{ii}[\text{cm}] = \frac{6.4T_e^2[\text{keV}]}{Z_i n_e[10^{21}\ \text{cm}^{-3}]} \tag{18}$$

(assuming $V_i/C_s = 5$), which depends only on the electron density and temperature and Z_i. For the case discussed above, where $n_e \sim 10^{22}$ cm^{-3}, one finds from (18) $\lambda_{ii} \sim 900\ \mu$m, consistent with Fig. 5(c). Equation (18) indicates that by varying n_e, one can make the interaction stronger or weaker. Figure 7 shows the results of a slightly different calculation in which the initial electron density has been increased to 3×10^{23} cm^{-3}; p_z-z ion phase space at $t = 1.2$ ns and the electron density profiles at several times are displayed. At the higher density, the ion mean free path is less. The plot shows that indeed the ions interact more rapidly over a shorter distance, which in this case leads to a large peak in n_e at $t = 1.8$ ns that correspond to the beginnings of two outward propagating shocks.

The same configuration also allows us to examine in detail other aspects of the model. For example, as discussed in Section IV, the intraspecies collision frequency, ν_α, is the limiting value of the interspecies collision frequency, $\nu_{\alpha\beta}$, when the relative drift between the species vanishes. One would then expect that if the two ion species were treated as a single species, the interaction that results from intraspecies collisions in this case should be similar to that from interspecies collisions between the two species. This expectation is born out in Fig. 8, which shows the results of the same run as in Fig. 5 at $t = 1.2$ ns, but all the ions are treated as one species interacting through intraspecies collisions. Ion phase space in the top panel indicates that the interaction is qualitatively similar to that in Fig. 5c concerning the degree of interpenetration as well as the heating and slowing of each ion beam. The bottom panel in Fig. 8 shows the corresponding electron density profiles in the two cases (solid curve, one ion species at $t = 1.2$ ns; dotted curve, two ion species); they are nearly identical.

While Fig. 8 showed the similarity of intraspecies collisions and interspecies collisions, Fig. 9 demonstrates the importance of including both effects. Again, two colliding plasma streams are considered (with the same parameters as Fig. 5). Ion p_z-z phase space at $t = 1.6$ ns is shown. In this case, however, the intraspecies collision term has been

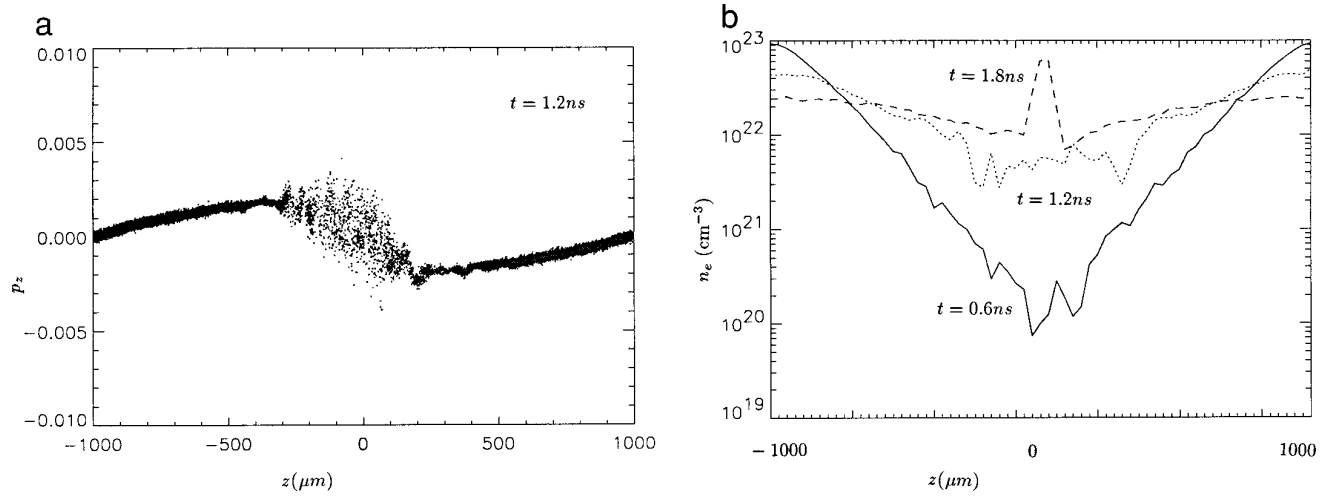

FIG. 7. One-dimensional calculation like that in Fig. 5, but with 10 times higher initial electron density: (top panel) $p_z - z$ phase space at $t = 1.2$ ns; (bottom panel) electron density profiles at three times.

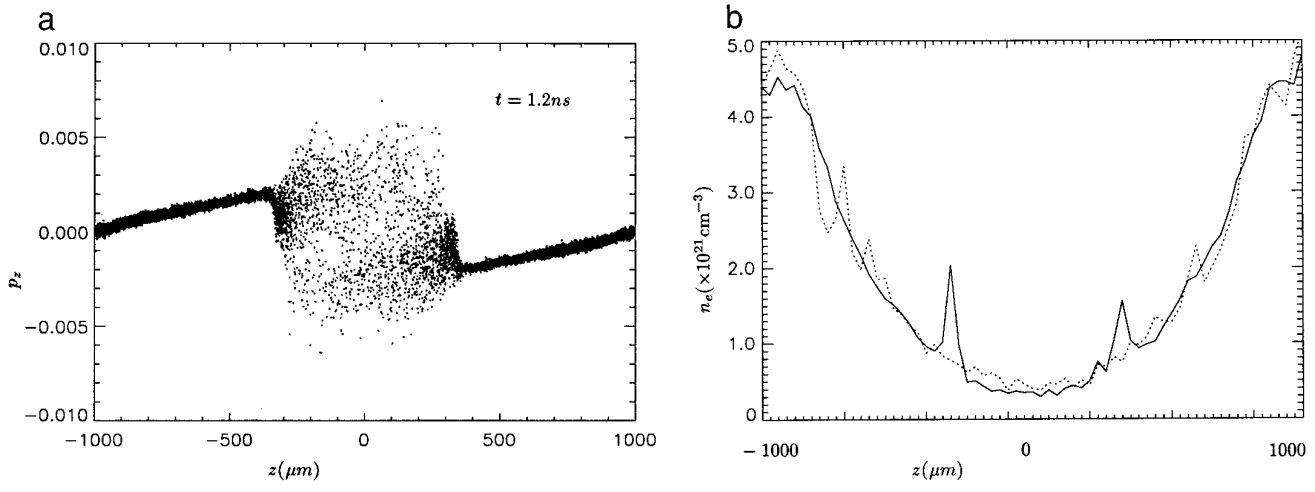

FIG. 8. Same calculation as in Fig. 5, but using only one ion species to represent ions from both targets that interact through intraspecies collisions only: (top panel) $p_z - z$ phase space at $t = 1.2$ ns; (bottom panel) electron density profile at same time (dotted curve corresponds to case in Fig. 5, solid curve corresponds to this run).

turned off. Note that like Fig. 5d, the ions of each species are slowed relative to each other over a similar interaction distance, but unlike the correct case, the ions here are heated relatively little. In addition, some ions are reflected back from the interaction region. Also, the incoming ions from each beam remain very cold and show oscillations that follow the fluctuations in the density. Evidently, intraspecies collisions are thus an important mechanism to thermalize the streams.

The method presented in this paper to treat particle collisions also works well for modeling the interaction of different materials; similar calculations have been carried out in [44]. Figure 10 shows p_z-z phase space at 1.2 ns for the expansion and interaction of laser heated gold foils (like Fig. 5, but 150 μm thick), but coated with 50 μm of CH (i.e., C^{+6} and H^+ ions with the total electron density of 3×10^{22} cm^{-3} in the coating, as well as in the gold slabs). The six panels correspond to p_z-z phase space for each of the six species used in the calculation. In this case the light H^+ ions expand more rapidly and because Z_i is small (Eq. (18)), they interpenetrate without much coupling. At the opposite slab, the ions are reflected by the electric field that initially accelerates the ions out of the foil. The heavier carbon ions expand somewhat slower, but like the hydro-

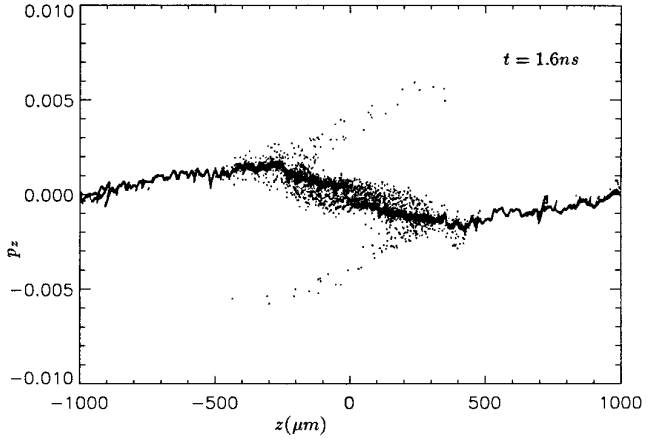

FIG. 9. Same calculation as in Fig. 5, but without intraspecies collisions, showing ion $p_z - z$ phase space at $t = 1.6$ ns.

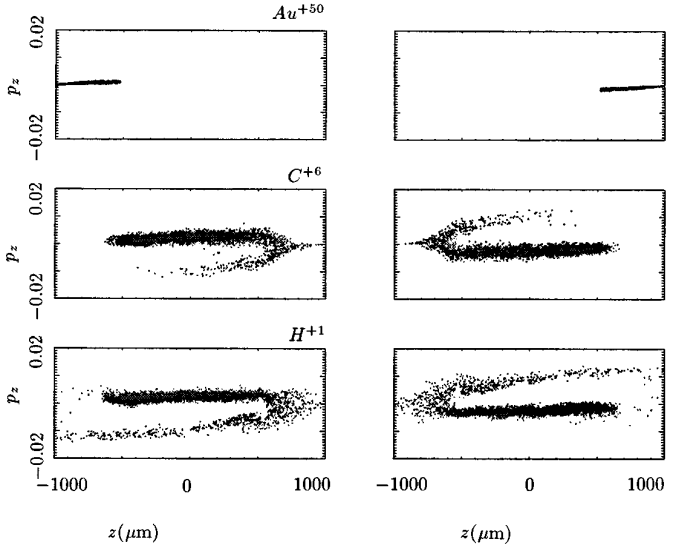

FIG. 10. Calculation like that in Fig. 5, but with gold target foils covered with CH coating. Ion phase space of all six species (Au, C, H) is shown at $t = 1.2$ ns.

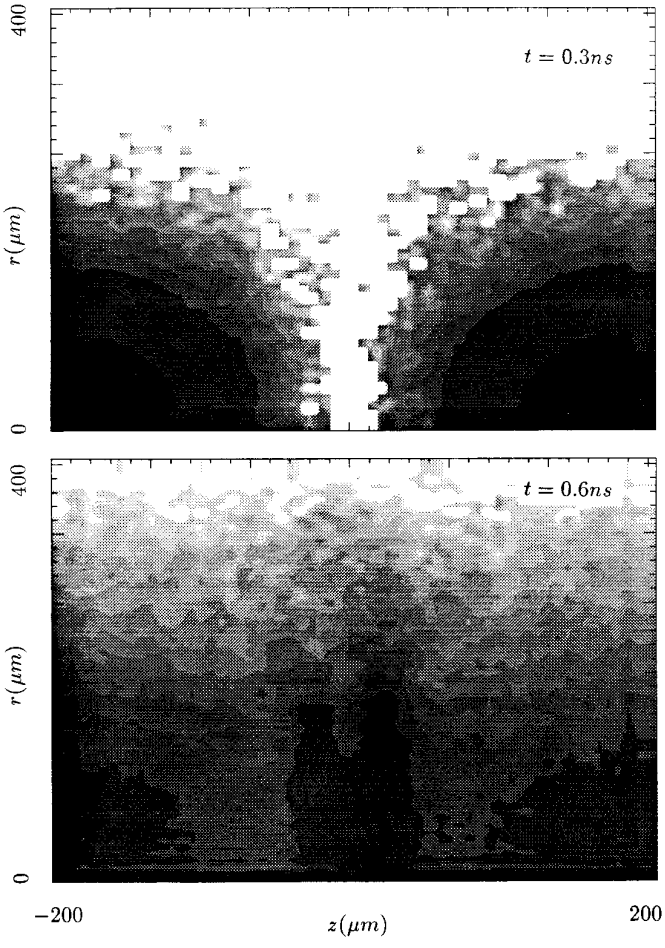

FIG. 11. Two-dimensional calculation of expanding plasmas (parameters given in text), showing electron density at $t = 0.3$ and 0.6 ns.

gen, the coupling according to Eq. (18) is still rather weak. The gold ions, on the other hand, are held back from interacting due to the interpenetration of the carbon and hydrogen ions.

The examples we have shown thus far in this section have involved one-dimensional calculations. As the examples in Sections III and IV have shown, the collision-field method actually works very well in two dimensions, where the grid-based nature of the scattering force is usually more efficient that by pairing up the particles in each cell (just as particle-in-cell methods are more efficient that charge sheet methods in two- and three-dimensional simulations (e.g., see [17])). To demonstrate a two-dimensional colliding plasma calculation, we show a final example in which the 30 μm gold slabs that are 340 μm apart also have a radius of 100 μm. In this case the computation grid is 60 (in z) $\times$ 60 (in r) and 40000 macroparticles are used to represent each of the gold ion species. Plotted in Fig. 11 are contour plots of the electron density (initially 10^{23} cm^{-3}) at two times, $t = 0.3$ and 0.6 ns. In this case, the expansion occurs in both z and r, leading to a somewhat small density in the center when the plasmas collide, with density peaks occurring on either side of the midplane.

VI. CONCLUSIONS

In this paper we have presented a new method for treating short-range Coulomb collisions between plasma species in particle codes. For interspecies collisions, the collision operator is based on the concept of a collision field, the form of which ensures that energy and momentum are conserved locally to a very good approximation even in the absence of a large number of particles per cell. For intraspecies collisions, the collision process is based on the Langevin equation. In both cases of collisions between different ion species and between ions of the same species, the form of the force is consistent with transport coefficients based on classical (Spitzer) processes. The method has been applied to ion–ion collisions, ion intraspecies collisions, and electron–ion collisions in a hybrid code that includes electromagnetic radiation effects. Numerical examples in both one and two spatial dimensions have been presented to show the validity and versatility of the approach. The model developed here provides a means to address the previously inaccessible region of semi-collisional plasmas. Particle-in-cell methods have proven effective for modeling collisionless plasmas and hydrodynamic or fluid models are equally effective for modeling the highly collisional regime. The collision force method incorporated in a hybrid code described in this paper shows considerable promise for modeling the intermediate regime and indeed bridging the gap between the collisionless and collisional regimes.

The collision field method is very efficient, represently an increase of only about 50% in computational burden over existing particle-in-cell methods, and allows the use of large time steps relative to the collision frequency. At present, the method is limited by a simplified electron energy model. However, we see no reason why more sophisticated models, e.g., including radiation transport, could not be incorporated, since the electrons are treated as a fluid and the methodology of energy transport in Eulerian fluids is well developed. Attempts at such improvements are presently underway. Similarly, at present the ion charge state is fixed, although in some applications of interest (laser matter interactions) a variable charge state would be more physically accurate. Because we have assumed quasineutrality and treat the electrons as a fluid, it may be possible to relax this constraint as well. Further development of other, more complex plasma–plasma and plasma–material interactions based on this formulation are also expected to occur, as needs arise in various applications.

APPENDIX A: ELECTROMAGNETIC HYBRID MODEL WITH RADIATION FIELDS

Hybrid simulation methods have become widespread in modeling low frequency plasma phenomena [3–14, 37]. The basic idea is to treat the electrons as a fluid, usually neglecting the electron mass, and to treat the ions by the particle-in-cell method. This method allows one to follow the dynamics of the plasma on the ion time scale, i.e., the ion gyroperiod in a magnetized plasma. The particle-in-cell method essentially solves the collisionless Boltzmann equation for the ions, giving a more complete description of the phase space evolution than a hydrodynamic model. Some approximations have been made that attempt to model the electron–ion collisional interaction [6], and ion–ion collisions have been treated through particle-pairing methods [34, 35]. As a result, hybrid methods, although suitable for following the time scales of interest, have not been optimally applied to high density collisional plasmas.

In what follows, we describe the basic equations of a new hybrid model and some of the unique features of its implementation. The method presented here is a simplified version of our previous hybrid formulation [7].

In general, the momentum equation for the electron fluid is

$$m_e\left(\frac{\partial \mathbf{v_e}}{\partial t} + \mathbf{v_e}\cdot\nabla\mathbf{v_e}\right) = -e\left(\mathbf{E} + \frac{\mathbf{v_e}\times\mathbf{B}}{c}\right) - \frac{\nabla(n_e k T_e)}{n_e} - m_e\sum_i \nu_{ei}(\mathbf{v_e} - \mathbf{v_i}), \tag{A.1}$$

where n_e is the electron density, T_e is the electron temperature, $\mathbf{v_e}$ and $\mathbf{v_i}$ are the electron and ion fluid velocities, $\mathbf{E}$ and $\mathbf{B}$ are the electric and magnetic field vectors, respectively; ν_{ei} is the electron–ion collision rate and m_e is the electron mass. In taking the limit of this equation as m_e vanishes, it is assumed that ν_{ei} becomes infinite so that the product $\nu_{ei}m_e$ remains finite. Furthermore, we will assume quasineutrality, which allows us to replace n_e with $\sum_i Z_i n_i$, the ion density.

Taking the limit as m_e goes to zero and using the quasineutral assumption, we thus obtain

$$\mathbf{E} = \frac{-\mathbf{J_e}\times\mathbf{B}}{\rho_e c} - \frac{\nabla(\rho_e k T_e)}{\rho_e e} - \frac{m_e}{e}\sum_i \nu_{ei}(\mathbf{v_e} - \mathbf{v_i}), \tag{A.2}$$

where the ion charge density $\rho_i = -\rho_e \equiv e n_e$ and $\mathbf{J_e}$ is the electron current density. In the usual hybrid approximation, this equation is solved for $\mathbf{E}$ assuming no displacement current. The magnetic field is then advanced in time by Faraday's law:

$$\frac{\partial \mathbf{B}}{\partial t} = -c\nabla\times\mathbf{E}. \tag{A.3}$$

There is typically a predictor corrector phase of the field calculation, because the current density depends on the magnetic field [5].

In the method presented here, the first term on the right-hand side of Eq. (A.2) is used separately to advance the magnetic field in a subcycling procedure. The electron current density in this equation is determined from Ampere's law neglecting the displacement current and is given by

$$J_e = \frac{c}{4\pi}\nabla\times\mathbf{B} - J_i. \tag{A.4}$$

In vacuum regions, the electric field is advanced with Ampere's law, including the displacement current:

$$\frac{\partial \mathbf{E}}{\partial t} = c\nabla\times\mathbf{B}. \tag{A.5}$$

These equations are subcycled to satisfy the vacuum Courant condition. This procedure correctly propagates electromagnetic waves in vacuum, and the resulting small time step eliminates the need for corrective time centering of the magnetic field. In many problems of interest, however, the magnetic field generated this way is small. In this limit, these terms can be neglected and subcycling is not necessary at all. After the subcycling in completed, the last two terms of Eq. (A.2) are added to the electric field and the corresponding magnetic field from Eq. (A.3) is also included. Using these electric and magnetic fields, the ions are treated in the usual particle-in-cell manner [2].

In the absence of magnetic fields, only the last two terms in Eq. (A.2) contribute. The first of these terms is the gradient of the electron pressure and is the usual force that one has in a hydrodynamic model. The last term in Eq. (A.2) represents a collisional drag term that for a single ion species can be balanced by the collisional force term discussed in Section III. However, for multiple ion species this term can give rise to a drag term on the ions that is usually not considered in hydrodynamics models.

The electron temperature T_e that enters into Eq. (A.2) can be determined in a number of different ways. The simpliest model assumes isothermal electrons; this approximation is valid for many laser applications. In general, an electron energy equation can be used to calculate the electron temperature. This equation can include electron–ion temperature coupling, electron–radiation coupling, heat transport, advection, and other sources and sinks for electron energy.

ACKNOWLEDGMENTS

This work was performed under the auspices of the U.S. Department of Energy. The authors thank Drs. R. L. Berger, A. Decoster, R. H. Miller, S. M. Pollaine, R. J. Procassini, and P. W. Rambo for useful discussions.

REFERENCES

1. J. P. Freidberg, *Ideal Magnetohydrodynamics* (Plenum, New York, 1987).
2. C. K. Birdsall and A. B. Langdon, *Plasma Physics via Computer Simulation* (McGraw–Hill, New York, 1985).
3. J. A. Byers, B. I. Cohen, W. C. Condit, and J. D. Hanson, *J. Comput. Phys.* **27,** 363 (1978).
4. D. W. Hewett and C. W. Nielson, *J. Comput. Phys.* **29,** 219 (1978).
5. D. S. Harned, *J. Comput. Phys.* **47,** 452 (1982).
6. A. G. Sgro and C. W. Nielson, *Phys. Fluids* **19,** 76 (1976).
7. M. E. Jones, V. A. Thomas, R. J. Mason, and D. Winske, ''A Fully Electromagnetic Hybrid Model for High Density Plasma Simulations,'' in *Proceedings, 13th Conf. on Numer. Simul. of Plasmas, Santa Fe, NM, Sept. 17–20, 1989* (unpublished).
8. D. Winske and N. Omidi, ''Hybrid Codes: Methods and Applications,'' in *Computer Space Plasma Physics: Simulation Techniques and Software,* edited by H. Matsumoto and Y. Omura (Terra Sci., Tokyo, 1993), p. 103.
9. R. J. Mason, *Phys. Rev. Lett.* **43,** 1795 (1979).
10. R. J. Mason, *Phys. Fluids* **23,** 2204 (1980).
11. R. J. Mason, ''Electron Transport Effects in Laser Produced Plasmas,'' in *Laser Interaction and Related Phenomena,* Vol. 5, edited by M. Lubin and B. Yaakobi (Plenum, New York, 1981).
12. R. J. Mason, *J. Comput. Phys.* **61,** 484 (1981).
13. R. J. Mason, ''Hybrid and Collisional Implicit Plasma Simulation Models,'' in *Multiple Time Scales,* edited by J. U. Brackbill and B. Cohen (Academic Press, New York, 1986), p. 233.
14. R. J. Mason and C. W. Cranfill, *IEEE Trans. Plasma Sci.* **PS-14,** 46 (1986).
15. O. Larroche, *Phys. Fluids B* **5,** 2816 (1993).
16. P. W. Rambo and J. Denavit, *J. Comput. Phys.* **98,** 317 (1992).
17. C. K. Birdsall, *IEEE Trans. Plasma Sci.* **19,** 65 (1991).
18. R. A. Bosch, R. L. Berger, B. H. Failor, N. D. Delameter, G. Charatis, and R. L. Kauffman, *Phys. Fluids B* **4,** 979 (1992).
19. R. Berger, J. R. Albritton, C. J. Randall, E. A. Williams, W. L. Kruer, A. B. Langdon, and C. J. Hanna, *Phys. Fluids B* **3,** 3 (1991).
20. D. W. Forslund and C. R. Shonk, *Phys. Rev. Lett.* **25,** 281 (1970).
21. N. Singh and J. L. Horwitz, *J. Geophys. Res.* **97,** 1049 (1992).
22. C. E. Rasmussen and R. W. Schunk, *J. Geophys. Res.* **93,** 14557 (1988).
23. G. R. Wilson, J. L. Horwitz, and J. Lin, *J. Geophys. Res.* **97,** 1109 (1992).
24. B. Coppi, M. N. Rosenbluth, and R. Z. Sagdeev, *Phys. Fluids* **10,** 582 (1967).
25. W. W. Lee, *J. Comput. Phys.* **72,** 243 (1987).
26. X. Q. Xu and M. N. Rosenbluth, *Phys. Fluids B* **3,** 627 (1991).
27. S. Ma, R. D. Sydora, and J. M. Dawson, *Comput. Phys. Commun.* **77,** 190 (1993).
28. A. M. Dimits and B. I. Cohen, *Phys. Rev. E.* **49,** 709 (1994).
29. R. A. Shanny, J. M. Dawson, and J. M. Greene, *Phys. Fluids* **10,** 1281 (1967).
30. P. Burger, *Phys. Fluids* **10,** 658 (1967).
31. J. M. Dawson, *Phys. Fluids* **7,** 419 (1964).
32. D. Montgomery and C. W. Nielson, *Phys. Fluids* **13,** 1405 (1970).
33. T. A. Oliphant and C. W. Nielson, *Phys. Fluids* **13,** 2103 (1970).
34. T. Takizuka and H. Abe, *J. Comput. Phys.* **25,** 205 (1977).
35. R. H. Miller and M. R. Combi, *Geophys. Res. Lett.* **21,** 1735 (1994).
36. L. Spitzer Jr., *Physics of Fully Ionized Gases* (Wiley Interscience, New York, 1962), p. 133.
37. J. M. Wallace, J. U. Brackbill, C. W. Cranfill, D. W. Forslund, and R. J. Mason, *Phys. Fluids* **30,** 1086 (1987).
38. K. D. Gibson and H. A. Scherega, *J. Comput. Chem.* **11,** 468 (1990).
39. U. Frisch, B. Hasslacher, and Y. Pomeau, *Phys. Rev. Lett.* **56,** 1505 (1986).
40. W. W. Roberts and M. A. Hausman, *Ap. J.* **277,** 744 (1984).
41. M. E. Jones, V. A. Thomas, and D. Winske, ''An Interparticle Collision Model for Electromagnetic Hybrid Simulations of High Density Plasmas,'' in *Proceedings, 14th Conf. on Numer. Simul. of Plasmas, Annapolis, MD, Sept. 3–6, 1991* (unpublished).
42. S. M. Pollaine, R. L. Berger, and C. J. Keane, *Phys. Fluids B* **4,** 989 (1992).
43. A. Decoster, private communication (Anomalous Absorption Conference, 1992).
44. P. W. Rambo and R. J. Procassini, *Phys. Plasmas,* **2,** 3130 (1995).
45. S. Chandrasekhar, *Rev. Mod. Phys.* **15,** 1 (1943).
46. D. S. Lemons, J. Lackman, M. E. Jones, and D. Winske, *Phys. Rev. E,* in press.
47. C. W. Cranfill, J. U. Brackbill, and S. R. Goldman, *J. Comput. Phys.* **66,** 239 (1986).
48. W. F. Noh, *J. Comput. Phys.* **72,** 78 (1988).